Available online at www.sciencedirect.com
SCIENCE DIRECT®
International Journal of Heat and Mass Transfer 49 (2006) 387–401
International Journal of HEAT and MASS TRANSFER
www.elsevier.com/locate/ijhmt

Microscopic analysis of interfacial electrothermal phenomena—definition of a heat generation factor

Grégory Le Meur, Brahim Bourouga *, Jean-Pierre Bardon

Ecole Polytechnique de l'Université de Nantes, Laboratoire de Thermocinétique—UMR CNRS 6607, Rue Christian Pauc, La Chantrerie—BP 90604, 44306 Nantes Cedex 3, France

Received 7 October 2003; received in revised form 22 October 2004
Available online 26 October 2005

Abstract

The thermal state at a solid–solid contact with interfacial heat generation requires the knowledge of two macroscopic contact parameters: the thermal contact resistance (R_{TC}) and the heat generation factor (α). R_{TC} is already well defined by many theoretical models, on the other hand, α remains poorly known and was never studied in the case of electrothermal contact. On the basis of a microscopic analysis of the coupled electrical and thermal phenomena in a current tube crossing two asperities in contact, we propose a model of the heat generation factor. This one is a combination of electrical resistivities and thermal conductivities of both materials in contact. Comparison of model to experimental data are presented and discussed.
© 2005 Elsevier Ltd. All rights reserved.

Keywords: Electrothermal contact; Joule effect; Interface; Heat generation factor; Analytical model; Constriction; Thermal contact resistance

1. Introduction

The thermal state at a solid–solid contact depends on the contact characteristics. In the hypothetical case of a perfect contact (Fig. 1, case a), the equations are well known: they are the temperatures continuity equation (1), and the conservation of heat flux transmitted by conduction through the interface.

When the contact is imperfect (interstitial defects, surface irregularities), the thermal field presents a discontinuity at the interface (Fig. 1, case b). Thus the condition (1) must be replaced by a homogeneous coupling condition of Fourier type (3), where the temperature discontinuity at the interface is proportional to the heat flux transmitted by conduction. The proportionality coefficient called thermal contact resistance (R_{TC}) characterises the thermal imperfection of the contact.

Finally, if the contact is imperfect and is the site of heat generation (sliding contact, electrothermal contact, ...), some difficulties appear due to heat generation and its location in the disturbed zone of the contact. The two coupling equations must be corrected. The correction of heat flux conservation is easy: the totality of the generated heat flux should be added to the flux transmitted by conduction through the interface. However, the discontinuity temperature condition is more difficult to modify. Keeping the notion of thermal contact

* Corresponding author. Tel.: +33 2 40 68 31 56; fax: +33 2 40 68 31 41.
E-mail address: brahim.bourouga@univ-nantes.fr (B. Bourouga).

0017-9310/$ - see front matter © 2005 Elsevier Ltd. All rights reserved.
doi:10.1016/j.ijheatmasstransfer.2005.02.029

Nomenclature

a	thermal diffusivity (m^2/s)	t	time (s)
I	current intensity (A)	T	temperature (K)
F	compression force (N)	U	voltage (V)
F	constriction function (m^{-1})	α	heat generation factor
k	proportionality coefficient between thermal resistance and resistive path	Γ	resistive path (K/W)
		ϕ_g	generated heat flux at the interface (W)
R	current tube radius (m)	λ	thermal conductivity (W/m K)
r_0	contact area radius (m)	ρ	density (kg/m^3)
R_c^e	electrical constriction resistance (Ω)	ρ	electrical resistivity (Ω m)
R_c^t	thermal constriction resistance (K/W)	θ	temperature (K)
R_{EC}	electrical contact resistance (Ω)	v	voltage (V)
R_{TC}	thermal contact resistance (K/W)		

resistance to characterise the imperfection of the contact, one have to answer the question: how taking into account the generated heat flux at the interface? Does it take part to the interfacial temperatures discontinuity in its entirety, partially or not at all? One must underline that none of the reference books about heat transfer treat this question [1–4]. On the other hand, the literature shows that many research works tackle that problem, but without an unanimously accepted formulation, authors propose various ways of writing that coupling condition (cf Section 2).

In the present work, we are particularly interested with electro-thermal contact. Like in the case of sliding contact, Joule effect heat generation at an electro-thermal contact is volumetric. The phenomenon is located on both sides of the theoretical contact plan, in the disturbed zone of the interface, thickness of which is about few tens microns. Heat flux which crosses this zone is non-conservative, and that property involves to add to R_{TC} another parameter α in the thermal coupling condition. This second parameter represents the generated heat flux fraction which takes part to the interfacial temperature discontinuity.

The goal of this study is to model α in the case of a static electro-thermal contact in thermal steady state. Nowadays, the growing rise of numerical simulation involves development of theoretical models describing α, following examples of those describing R_{TC} [54–56]. The paper is organized in three sections. In the first one, we present an over review about thermal coupling conditions at interfaces which are the site of heat generation. In the second one the model describing α is developed. The third part is devoted to the comparison of the model with experimental results.

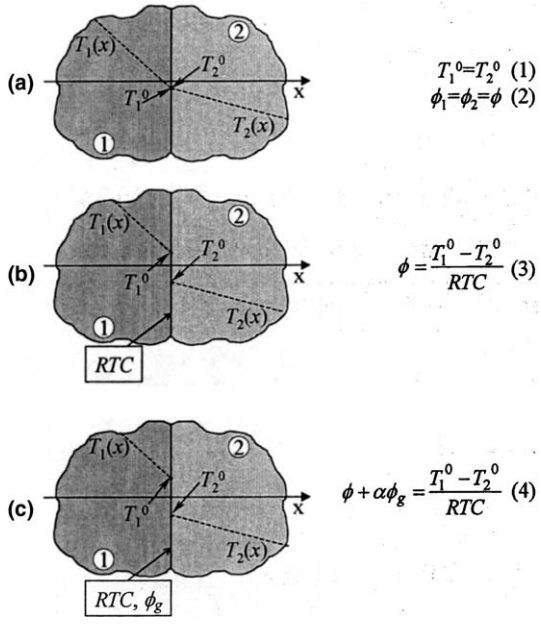

Fig. 1. Equations of the thermal contact condition versus contact characteristics.

2. An over review of thermal contact condition with heat generation

Most of works are about contacts which are the site of mechanical heat generation (sliding contact, machining, grinding, ...). The first description of the generated heat flux partition at a sliding contact was proposed by Vernotte [5]. The author considers a transient contact problem involving frictional heat generation between two semi-infinite media. The contact is assumed to be perfect and the frictional generated heat flux is partitioned between the two contacting bodies according to their thermal effusivities. In their theoretical models, Kato [6] and Chadrasekar [7] used that formulation of the coupling condition in the case of a grinding problem.

Their results were in good agreement with the experimental results of Grzesik [8]. However, that formulation of the coupling condition remains valid only for the short time scales (case of the hypothesis of semi-infinite medium). It is not usable in thermal steady state [9,10].

Several works about sliding contact present analytical method to solve thermo-elasticity problems [11–23]. Generally, those problems are related to one conducting medium sliding on a non-conducting body. In that situation, the thermal contact condition is based on two assumptions: the contact is perfect and the totality of the generated heat flux is absorbed by the conducting body. That is a limit case of Ref. [5], which is valid what ever the time scale. However, the perfect contact assumption between two bodies in sliding contact was put at fault by Dimarogonas [24] who experimentally showed the existence of a temperature difference between the two surfaces in contact of a brake disc.

Still in the case of sliding contact, Varadi [25] numerically simulates the elastoplastic deformations of two surfaces in friction. Asperities in contact are considered as semi-infinite media in thermal steady state. The generated heat flux at the contact points is partitioned according to the thermal conductivity of materials in contact. Kulchytsky [26] also used that definition while using a corrective term related to the contact cooling by convection.

Komanduri [27–29] proposes analytical solutions of several applications of sliding contact (bearings, machining). The method used consists in coupling analytical solutions of a solid heated by a moving heat source with that of a solid heated by a stationary heat source of the same geometry [1]. The author shows that a solution exists only if heat flux partition along the interface is non-uniformly distributed.

Levytsky [30,31] and Yevtushenko [32] propose analytical solutions to many thermo-elasticity problems of sliding contacts. They take into account the thermal contact resistance and localize the heat generation on the theoretical contact area, which is the site of the most important heating of the system. Consequently, the generated heat flux is partitioned into two parts, each one crossing one of the disturbed zones of the contact. Other authors like Ciavarella [33] localize the heat generation on one of the two frictional surfaces which is the site of the most important heating of the system. That modelling implies that only one part of the generated heat flux crosses the thermal contact resistance in its entirety.

Those modellings of heat generation locations are always non-justified, so they do not take into account the complexity of heat generation phenomena. Currently, it is well known that heat generation at a sliding contact is due to two types of heat sources. The first one is volumetric and is due to plastic deformations in the sheared zone of the contact. The second one is surfacic and is due to the friction between the two bodies in contact [8]. It is necessary to localise precisely the heat sources to define adequately the parameter which, in addition with R_{TC}, intervenes in the interfacial coupling condition [34–36].

The consideration of volumetric heat sources in the case of sliding contacts leads to formulate the interfacial coupling condition in a different way. Bardon [37] proposed that the partition coefficient of interfacial generated heat flux can be replaced by the notion of "part of the generated heat flux which contributes to the interfacial temperature discontinuity". That concept has the merit to consider the non-conservative character of the heat flux which crosses the perturbed zone of the contact. That notion was adopted by Chantrenne [38] who proposes a thermal model of the sliding contact taking into account a volumetric heat generation at the interface. That model is based on a microscopic analysis of heat transfers and generation phenomena in the vicinity of the interface. A numerical procedure allows to determine the sliding thermal contact resistance and α starting from a microscopic model. That study shows that α depends on heat sources locations near the interface. Influence of the contact geometry on α and R_{TC} was also highlighted.

Laraqi [39] proposes an approach of frictional heat generation based on a Gaussian distribution of heat sources. However, the problem involving in heat sources intensities characterization remains posed. The author shows influence of heat transfers between the contact and its surrounding on α, and thus concludes that α is not an intrinsic property of the interface.

In recent studies, Bauzin [40,41] presented experimental results of simultaneous estimations of α, ϕ_g and R_{TC} in the case of sliding contact. His results show that the thermal coupling condition is well defined by the two parameters R_{TC} and α. In addition, experiments on notched samples permitted to show that α can be determined from constriction resistances measurements. Values of α obtained by this way are in good agreement with estimated values by inverse analysis. Finally, Bauzin observed that α is correlated with materials effusivities beyond a sliding velocity threshold. On the other hand, R_{TC} is not very sensitive to that parameter.

Whether the authors are mechanical or heat engineers, it arises that works which aim at defining the sliding contact coupling condition runs up against the problem of the precise localization of heat generation zones. This problem does not arise in the case of electro-thermal contact which offers the advantage of the precise knowledge of the heat sources distribution starting from the solution of the electric problem [42–44]. Paradoxically, in the case of electro-thermal contact, the macroscopic thermal aspects were studied very little and few works concerned the thermal coupling condition [45,46]. The main part of studies close to the subject were about electricity of power, and in particular the spot

welding process application, the study of which is justified by the growing rise of numerical simulation in the industrial community. So, in the electrode–sheet interface study, Cho [47] and Han [48] neglect the thermal contact resistance and the interfacial generated heat flux by Joule effect. In another study, Cho [49] takes into account the interfacial generated heat flux in the heat balance but neglects the contact imperfection. In a recent numerical study, Khan [50] considers R_{TC} at electrode–sheet interface but neglects the interfacial generated heat flux. Finally, Wang [51] considers those two properties of electro-thermal contact. The author considers that the generated heat flux, negligible compared to heat flux transmitted by external heat sources, does not take part to the interfacial temperature discontinuity. Recently, Le Meur et al. estimated simultaneously R_{TC} and α during a resistance spot welding operation by implementing a very fine thermocouple instrumentation and an adapted inverse problem resolution [52,53].

In summary it appears that without an unanimously accepted formulation, the thermal coupling condition at an interface which is the site of heat generation was approached in very different ways according to authors'. In the majority of these studies, the coupling condition is formulated in a simplified way without taking into account the real physical nature of interfacial heat generation phenomena. This work aims at filling this gap, at least in the case of electro-thermal contact.

3. The current tube model

In order to account for the electro-thermal diffusion phenomena which hold in the disturbed zone of the contact, we proposed a model of an electric current tube crossing two asperities of different materials in contact [57]. This model consists of two cylinders of the same radius R and of the same axis, in partial contact on a disc of radius r_0.

The side surface of the cylinders is electrically and thermally insulated to ensure current and heat conservation. Two zero temperatures are imposed at the external boundaries. The heat generation due to Joule effect is the only source term considered to highlight thermal phenomena which are the consequence of superposition of the fully developed electric and thermal constrictions around an elementary contact spot (Fig. 2). The mathematical formulation of the diffusion problem is given by the following set of equations.

Electrical problem:

$$\Delta V_i = 0; \quad i = 1,2; \quad -l_1 < z < l_2; \quad 0 < r < R \tag{5.1a}$$

$$V_1(r,-l_1) = 0; \quad 0 < r < R \tag{5.1b}$$

$$\sigma_1 \frac{dV_1}{dz}(r,0) = \sigma_2 \frac{dV_2}{dz}(r,0); \quad 0 < r < r_0 \tag{5.1c}$$

$$V_1(r,0) = V_2(r,0); \quad 0 < r < r_0 \tag{5.1d}$$

$$\frac{dV_1}{dz}(r,0) = \frac{dV_2}{dz}(r,0) = 0; \quad r_0 < r < R \tag{5.1e}$$

$$V_2(r,l_2) \neq 0; \quad 0 < r < R \tag{5.1f}$$

$$\frac{dV_1}{dr}(0,z) = \frac{dV_2}{dr}(0,z) = 0; \quad -l_1 < z < l_2 \tag{5.1g}$$

$$\frac{dV_1}{dr}(R,z) = \frac{dV_2}{dr}(R,z) = 0; \quad -l_1 < z < l_2 \tag{5.1h}$$

Thermal problem:

$$\Delta T_i = -\sigma_i (\mathrm{grad}\, V_i)^2; \quad i = 1,2; \quad -l_1 < z < l_2; \quad 0 < r < R \tag{5.2a}$$

$$T_1(r,-l_1) = 0; \quad 0 < r < R \tag{5.2b}$$

$$\lambda_1 \frac{dT_1}{dz}(r,0) = \lambda_2 \frac{dT_2}{dz}(r,0); \quad 0 < r < r_0 \tag{5.2c}$$

$$T_1(r,0) = T_2(r,0); \quad 0 < r < r_0 \tag{5.2d}$$

$$\frac{dT_1}{dz}(r,0) = \frac{dT_2}{dz}(r,0) = 0; \quad r_0 < r < R \tag{5.2e}$$

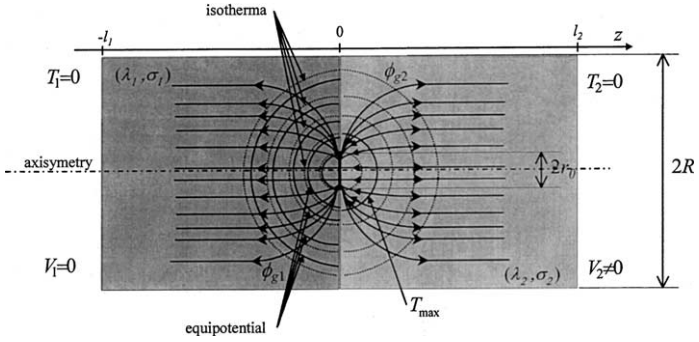

Fig. 2. The current tube model.

$$T_2(r, l_2) = 0; \quad 0 < r < R \tag{5.2f}$$

$$\frac{dT_1}{dr}(0, z) = \frac{dT_2}{dr}(0, z) = 0; \quad -l_1 < z < l_2 \tag{5.2g}$$

$$\frac{dT_1}{dr}(R, z) = \frac{dT_2}{dr}(R, z) = 0; \quad -l_1 < z < l_2 \tag{5.2h}$$

The resolution of coupled electrical and thermal equations is done numerically using a finite volumes scheme of discretization. The numerical grid is non-uniform. It has been refined around the contact area boundary because it is the location of large electrical and thermal gradients.

A typical numerical result is shown in Fig. 3, in the case of two platinum and copper media. Note that the maximum isotherm and the largest thermal gradient is located in the Pt cylinder. For other couples of materials, on observed that the bigger the electrical resistivities ratio is, the more the maximum isotherm is far from the interface in the more resistive medium. The maximum isotherm delimits a volume with the contact area. The generated heat in that volume contributes to the heating of medium 2 that it crosses in its entirety.

This simple model permits to show the particular characteristics of the electrical and thermal fields, which prevail in the disturbed zone, in the vicinity of the interface.

3.1. Discussion about the partition of the generated heat flux at the interface

If the radius R of the current tube is very large in front of the radius r_0 of the contact disc ($r_0 < R/10$) areas on the both sides of the contact can be regarded as two

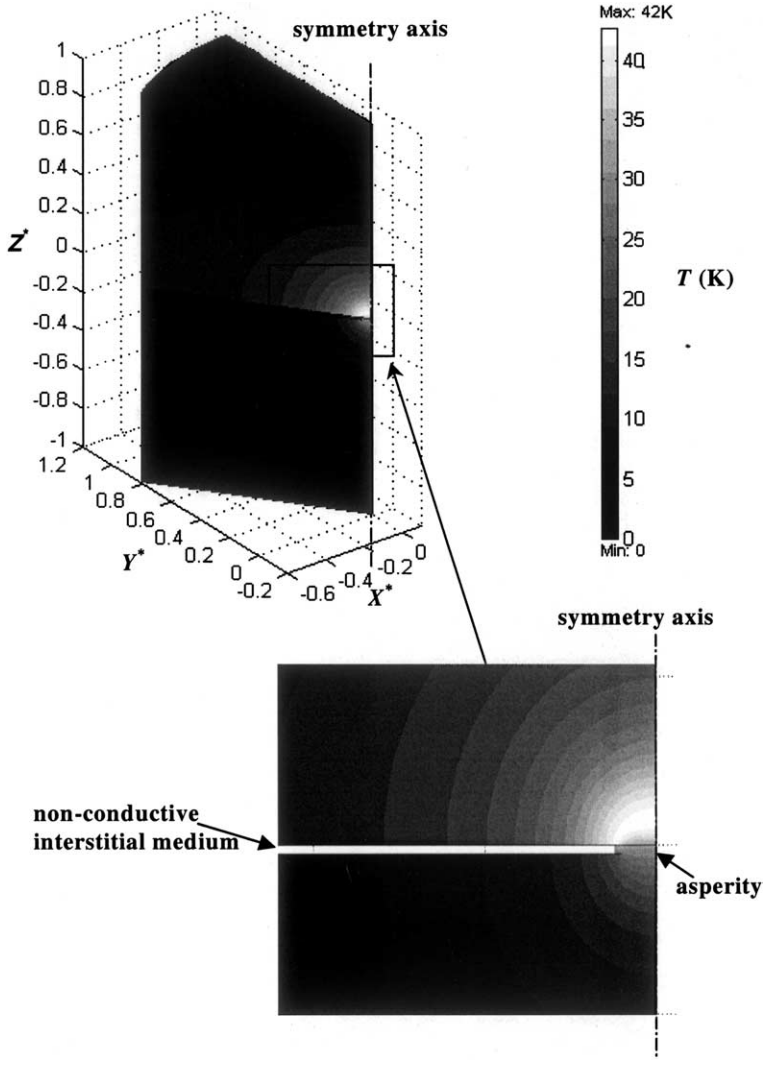

Fig. 3. A numerical solution of the current tube model—contact platinum/copper.

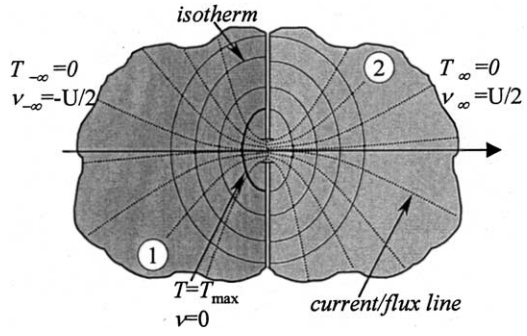

Fig. 4. Model of two semi-infinite media in partial contact.

semi-infinite media in partial contact on a disc of radius r_0, with two zero temperatures imposed on the boundaries (in $z \to \pm\infty$) (Fig. 4).

The maximum isotherm is an adiabatic surface localised in medium 1 (platinum) which, by convention, is the most electrically and thermally resistive. It shares the generated heat flux in the medium 1 in two parts. One of them flows toward the boundary of medium 1, and the other crosses the contact disc ($z = 0$) and flows towards the boundary of medium 2 (in $z \to \pm\infty$). Consequently, T_{max} satisfies the relation:

$$T_{max} = \phi_{g1}^{left} \Gamma_1^{left} = \phi_{g1}^{right}(\Gamma_1^{right} + R_{c2}) + \phi_{g2}\Gamma_2 \tag{6}$$

ϕ_{g1}^{left} and ϕ_{g1}^{right} respectively represent the generated heat flux on the left and on the right of the maximum isotherm in medium 1. ϕ_{g2} represents the generated heat flux in medium 2. Γ_1^{left} and Γ_1^{right} are what we call "resistive paths". Even if they are of the same dimension, they are not exactly thermal resistances because of the non-conservative character of the heat flux due to the volumetric heat generation. These resistive paths represent the average of the resistive journeys covered by elementary quantities of heat generated in medium 1, from the place where they are generated to the boundaries ($z \to -\infty$ or $z = 0$) where they end up.

In the same way, Γ_2 represents the resistive path in medium 2 crossed by ϕ_{g2}. Γ_1^{left} and Γ_1^{right} are respectively at the origin of the temperature variations $T_{max} - T_{-\infty} = T_{max}$ and $T_{max} - T_0$ in medium 1. T_0 is the temperature of the contact disc with radius r_0. R_{c2}^t is the thermal constriction resistance in medium 2.

3.2. Relation between resistive path and thermal resistance

One starts from a relation between the voltage field v and the temperature field θ in an electro-thermal constriction established by Holm [42]. That relation established for two media of the same material in contact is valid what ever the geometry of the interface (one or several contact areas). It is established assuming the constant thermal conductivity λ_0 and the electrical resistivity ρ_0. It is written as:

$$v^2 = 2\rho_0\lambda_0[T_{max} - \theta] \tag{7}$$

If one considers two semi-infinite media of the same material in contact, between the boundaries of which one imposes a voltage difference U ($v_{-\infty} = -U/2$ and $v_{+\infty} = +U/2$), and temperatures $T_{\pm\infty} = 0$, the limit of expression (7) when $z \to \pm\infty$ is written as:

$$U^2/4 = 2\rho_0\lambda_0 T_{max} \tag{8}$$

The generated heat flux in each electric constriction is:

$$\phi_g = \frac{U^2/4}{R_c^e} \tag{9}$$

Eq. (8) in (9) gives:

$$\phi_g = \frac{2\rho_0\lambda_0 T_{max}}{R_c^e} \tag{10}$$

The constriction function F is the same in the electrical and thermal problems when there is no volumetric heat generation, so:

$$F = R_c^e/\rho_0 = \lambda_0 R_c^t \tag{11}$$

These electric and thermal constriction resistances are linked by:

$$R_c^e = \rho_0\lambda_0 R_c^t$$

Thus (10) can be written as:

$$\frac{\phi_g}{2} = \frac{T_{max}}{R_c^t} \quad \Longleftrightarrow \quad T_{max} = \frac{R_c^t}{2}\phi_g \tag{12}$$

Expression (12) shows that, in a medium with Joule effect heat generation (unconservative heat flux), the temperature difference between the maximum and the minimum (zero) isotherms is proportional to ϕ_g and to the half of the thermal resistance between the two isotherms when the medium is not the site of heat generation. According to the definition of the resistive path Γ, one can write:

$$T_{max} = \Gamma\phi_g \tag{13}$$

By identification, the resistive path Γ is equal to the half of the thermal resistance R between the boundaries of the medium when there is no heat generation:

$$\Gamma = \frac{1}{2}R \tag{14}$$

If one denotes R_{c1}^e the electrical constriction resistance in medium 1 between $z = 0$ and $z \to -\infty$, and R_{g1}^e and R_{d1}^e the parts of this resistance respectively located on the left and on the right of the equipotential associated to the maximum isotherm, one can write:

$$\phi_{g1} = R_{c1}^e I^2 \quad \phi_{g1}^{left} = R_{g1}^e I^2 \quad \text{and} \quad \phi_{g1}^{right} = R_{d1}^e I^2 \tag{15}$$

where I is the current intensity which crosses the contact area.

One can deduce the fractions of the generated heat flux flowing on the left and on the right of the maximum isotherm:

$$\gamma = \frac{\phi_{g1}^{left}}{\phi_{g1}} = \frac{R_{g1}^{e}}{R_{c1}^{e}} \quad \text{and} \quad 1-\gamma = \frac{\phi_{g1}^{right}}{\phi_{g1}} = \frac{R_{d1}^{e}}{R_{c1}^{e}} \tag{16}$$

The parts R_{g1}^{t} and R_{d1}^{t} of the thermal constriction resistance R_{c1}^{t} in medium 1, located on the left and on the right of the maximum isotherm verify then the same expressions:

$$\gamma = \frac{R_{g1}^{t}}{R_{c1}^{t}} \quad \text{and} \quad 1-\gamma = \frac{R_{d1}^{t}}{R_{c1}^{t}} \tag{17}$$

Then, starting from relation (14), it is possible to express the thermal resistive paths Γ_1^{left}, Γ_1^{right}, and Γ_2 according to the thermal constriction resistances:

$$\Gamma_1^{left} = \frac{1}{2}R_{g1}^{t} = \frac{1}{2}\gamma R_{c1}^{t} \tag{18}$$

$$\Gamma_1^{right} = \frac{1}{2}R_{d1}^{t} = \frac{1}{2}(1-\gamma)R_{c1}^{t} \tag{19}$$

$$\Gamma_2 = \frac{1}{2}R_{c2}^{t} \tag{20}$$

Now let us use the results of this microscopic analysis to define α at the macroscopic scale.

3.3. Definition of coefficient α

3.3.1. General case

Let us consider an electrothermal contact between two different media (Fig. 5). The interface is considered here at the macroscopic scale, i.e. the thickness of the perturbed zone of the contact is considered zero. The external boundaries of the two elements in contact are submitted to two different temperatures T_{-L1} and T_{L2}. Thus, the thermal contact condition is written as:

$$\phi_1 + \alpha\phi_g = \frac{T_1 - T_2}{R_{TC}} \tag{21}$$

in addition with a heat flux conservation equation. The interfacial temperature discontinuity is due to the crossing of the transmitted heat flux ϕ_1 and of a fraction α of the generated heat flux ϕ_g through R_{TC}.

It is convenient to represent the interfacial heat transfers phenomena by a thermal resistive scheme between temperatures T_1 and T_2 (Fig. 6). Where β is the part of total heat flux generated in medium 1, and k_i are the proportionality coefficients between thermal resistances and resistive paths, i.e. the fractions of thermal contact resistances which take part to the interfacial temperature discontinuity. R_{TC1} and R_{TC2} are the two fractions of R_{TC} assigned respectively on the left and on the right sides of the interface ($R_{TC} = R_{TC1} + R_{TC2}$).

Eq. (21) expresses that heat flux ϕ_1, transmitted from body 1, crosses the entire thermal contact resistance. On the other hand, generated heat flux ϕ_g does not take part in its entirety to the temperature discontinuity $T_1 - T_2$; that is due to the non-conservative character of ϕ_g. As it has been previously shown, that amounts to saying that heat flux $\beta\phi_g$ and $(1-\beta)\phi_g$, generated respectively on the sides 1 and 2, cross only fractions $k_1 = k_2 = 1/2$ of the thermal contact resistances R_{TC1} and R_{TC2}. Temperatures T_{i1} and T_{i2} are fictitious temperatures, necessary for the representation of the thermal resistive scheme; they have no physical reality.

Thus, the interfacial temperature discontinuity is written as:

$$T_1 - T_2 = (1-k_1)R_{TC1}\varphi_1 + (k_1R_{TC1} + (1-k_2)R_{TC2}) \times (\beta\varphi_g + \varphi_1) + k_2R_{TC2}(\varphi_g + \varphi_1) \tag{22}$$

$$T_1 - T_2 = \varphi_1[R_{TC1} + R_{TC2}] + \varphi_g[\beta(k_1R_{TC1} + (1-k_2)R_{TC2}) + k_2R_{TC2}]$$

$$\varphi_1 + \varphi_g\left[\left(\beta\frac{k_1R_{TC1} + (1-k_2)R_{TC2}}{R_{TC1} + R_{TC2}}\right) + k_2\frac{R_{TC2}}{R_{TC1} + R_{TC2}}\right] = \frac{T_1 - T_2}{R_{TC}} \tag{23}$$

By comparing Eqs. (21) and (23), one obtains the expression of α:

$$\alpha = \beta\frac{k_1R_{TC1} + (1-k_2)R_{TC2}}{R_{TC1} + R_{TC2}} + k_2\frac{R_{TC2}}{R_{TC1} + R_{TC2}} \tag{24}$$

By replacing k_1 and k_2 by 1/2 one obtains:

$$\alpha = \frac{1}{2}\left(\beta + \frac{R_{TC2}}{R_{TC1} + R_{TC2}}\right) \tag{25}$$

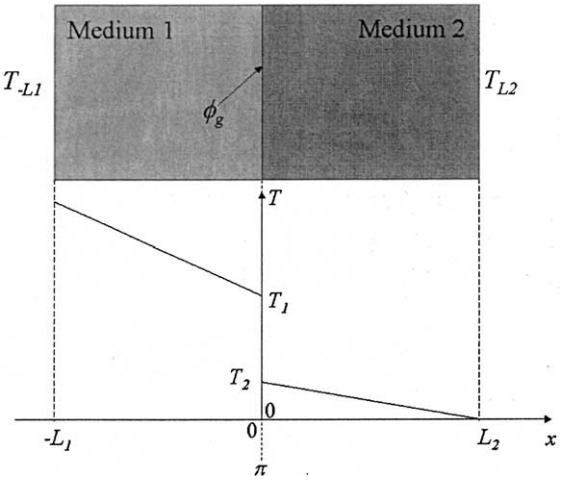

Fig. 5. Macroscopic contact.

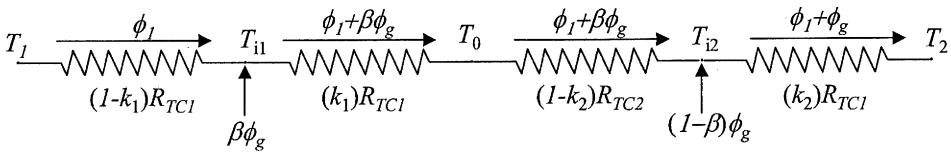

Fig. 6. Thermal resistive scheme—general case.

Lastly, since $\beta = \frac{\rho_1}{\rho_1+\rho_2}$, and $\frac{R_{TC2}}{R_{TC1}+R_{TC2}} = \frac{\lambda_1}{\lambda_1+\lambda_2}$:

$$\alpha = \frac{1}{2}\left(\frac{\rho_1}{\rho_1+\rho_2} + \frac{\lambda_1}{\lambda_1+\lambda_2}\right) \tag{26}$$

The expression of α is obtained from a particular formulation of the thermal coupling condition (22). This last distinguishes the contributions of the transmitted heat flux ϕ_1 and of the interfacial generated heat flux ϕ_g to the contact temperature discontinuity. Knowing that ϕ_1 is expressed from the gradient at the interface, α does not depend on thermal boundary conditions. In addition, expression (26) calls upon the Holm's law which is independent of the contact geometry. So α does not depend either on the interface structure, α is a combination of the thermophysical properties of the materials playing a role in the generation and heat transfer phenomena in the interfacial zone.

Expression (26) is based on the assumption of constant thermo-physical properties. In the more realistic case where thermo-physical properties ρ_i and λ_i depend on temperature, relation (26) remains valid provided that one evaluates those properties at the average temperatures of surfaces in contact (an iterative procedure would be necessary in that case).

Although the geometrical characteristics of the contact do not explicitly appear in expression (26), these last have an indirect influence on α. Indeed, the geometrical imperfection of the contact, at the origin of R_{TC} and R_{EC} (i.e. ϕ_g), generates a temperature jump at the interface which sets values of electrical resistivities and thermal conductivities of which depends α.

To highlight that α is independent from the external boundary conditions, let us consider the same analysis in the particular case where two zero temperatures are imposed at the external boundaries.

3.3.2. Case of two zero temperatures imposed at the external boundaries

In the particular case where two zero temperatures are imposed at the external boundaries, heat transfers can be represented by the thermal resistive scheme in Fig. 7.

In this case, the thermal contact condition (21) remains valid, but ϕ_1 depends on ϕ_g. The interfacial temperature discontinuity can be expressed as follows:

$$T_1 - T_{i1} = -\varphi(1-k_1)R_{TC1} \tag{27}$$

$$T_{i1} - T_{i2} = [k_1 R_{TC1} + (1-k_2)R_{TC2}](-\varphi_1 + \beta\varphi_g) \tag{28}$$

$$T_{i2} - T_2 = k_2 R_{TC2}(-\varphi_1 + \varphi_g) \tag{29}$$

By adding these three equations one obtains:

$$T_1 - T_2 = -\phi_1(R_{TC1} + R_{TC2}) + [k_1 R_{TC1} + (1-k_2)R_{TC2}]\beta\phi_g + k_2 R_{TC2}\phi_g \tag{30}$$

So, the thermal contact condition (21) can be written as:

$$-\varphi_1 + \frac{k_2 R_{TC2} + \beta[k_1 R_{TC1} + (1-k_2)R_{TC2}]}{R_{TC}}\phi_g = \frac{T_1 - T_2}{R_{TC}} \tag{31}$$

By replacing k_1 and k_2 by 1/2, and since $\beta = \frac{\rho_1}{\rho_1+\rho_2}$, and $\frac{R_{TC2}}{R_{TC1}+R_{TC2}} = \frac{\lambda_1}{\lambda_1+\lambda_2}$, one obtains:

$$\alpha = \frac{1}{2}\left(\frac{\rho_1}{\rho_1+\rho_2} + \frac{\lambda_1}{\lambda_1+\lambda_2}\right) \tag{32}$$

Whatever the thermal boundary conditions, α has always the same expression (26) depending on the thermophysical properties of materials in contact which govern heat generation and transfers. α is an intrinsic property of the interface.

Let us compare now the values of experimental estimations of α with those obtained starting from the theoretical model.

4. Experimental study: estimation of R_{TC} and α

Results presented in this section concern experiments undertaken in unsteady state. However, the characteristic time of electric and thermal constrictions phenomena being very short (~1 μs for the thermal problem, and

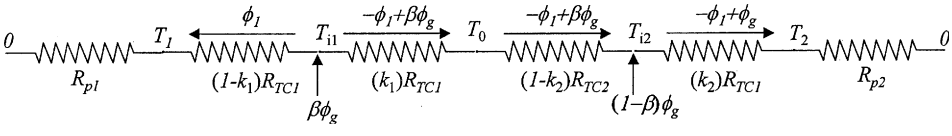

Fig. 7. Thermal resistive scheme—case of two zero temperatures imposed at external boundaries.

shorter for the electric one), and quite lower than the experiments durations, the previous definition of α (26) remains valid in these applications. We have developed and constructed two different experiments. The first one is developed in laboratory and concern the case of static contact between two metallic cylinders crossed by an electrical current [46]. The second one, carried out in an industrial environment, is related to the spot welding process, and more especially to the dynamic electrode–sheet contact [52]. Before the comparison between the values given by the theoretical model (26) and the ones obtained by experiments, we present the experimental setups.

4.1. Case of a static contact

4.1.1. Measurement principle

Coefficient α has been estimated simultaneously with R_{TC} in the case of a static electro-thermal contact. The measurement principle is based on the analysis of the transient thermal field in two copper and steel cylinders in contact heated by Joule effect. The measurement principle is schematically presented in Fig. 8. The two cylinders are assembled between two water boxes, aligned and tightened by means of a press which applies a normal force F to them. They can be crossed by a heat flux and/or an electrical current. The electrical current is provided by a stabilized power supply connected at the two ends of the cylinders (electrodes A and B). The heat flux is provided by the water boxes carrying two water flows maintained at two different (or equal) temperatures θ_1 and θ_2. The side surface is thermally insulated.

The contact located at $x = 0$ is imperfect. So, it is the site of an electrical contact resistance which opposes to the electric current and of a thermal contact resistance which opposes to the heat flux. The electrical contact resistance noted R_{EC} is supposed to be known starting from an auxiliary measurement [62]. It is used to calculate the generated heat flux density ϕ_g (W/m^2) at interface $x = 0$ when an electrical current crosses the contact. In the same way, the thermophysical characteristics of both materials are assumed to be well known, in particular the electrical resistivities which are used to calculate the volumetric heat sources P_1 and P_2 (W/m^3) (Table 1) [60,61].

Table 1
Materials properties

Materials	Steel	Copper
λ (W/m K)	40	320
ρ (nΩ m)	100	50

With such a device, the estimation of R_{TC} and α can be carried out by means of a 1D transient linear conductive model defined on the domain $[-L_1; L_2]$ for $t > 0$, and by the measurement of temperatures at selected points of the cylinders axis. Points $x = -L_1$ and $x = L_2$ are equipped with thermocouples which record temperatures $T_{-L1}(t)$ and $T_{L2}(t)$ respectively. Thus, we consider boundary conditions of the first kind at these two points. The linear system describing the heat transfer in the device can be formulated as follows:

$$\frac{1}{a_1}\frac{\partial T_1}{\partial t} = \frac{\partial^2 T_1}{\partial x^2} + \frac{P_1}{\lambda_1} \quad -L_1 \leqslant x \leqslant 0, \quad t > 0 \tag{33a}$$

$$\frac{1}{a_2}\frac{\partial T_2}{\partial t} = \frac{\partial^2 T_2}{\partial x^2} + \frac{P_2}{\lambda_2} \quad 0 \leqslant x \leqslant L_2, \quad t > 0 \tag{33b}$$

$$T_1(-L_1, t) = T_{-L_1}(t) \quad x = -L_1, \quad t > 0 \tag{33c}$$

$$\lambda_1 \frac{\partial T_1(0^-, t)}{\partial x} = \lambda_2 \frac{\partial T_2(0^+, t)}{\partial x} + \varphi_g \tag{33d}$$

$$\lambda_2 \frac{\partial T_2(0^+, t)}{\partial x} + \alpha\varphi_g = \frac{T_2(0^+, t) - T_1(0^-, t)}{R_{TC}} \tag{33e}$$

$$T_2(L_2, t) = T_{L_2}(t) \quad x = L_2, \quad t > 0 \tag{33f}$$

$$T_1(x, 0) = T_i^1(x) \quad -L_1 \leqslant x \leqslant 0, \quad t = 0 \tag{33g}$$

$$T_2(x, 0) = T_i^2(x) \quad 0 \leqslant x \leqslant L_2, \quad t = 0 \tag{33h}$$

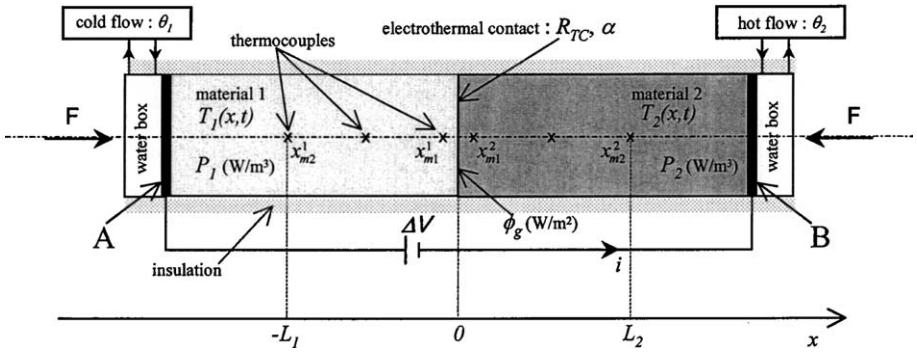

Fig. 8. Measurement principle.

where $T_i^j(x)$ $(j = 1,2)$ represent the initial temperature distribution in the domain $[-L_1, L_2]$ before the passage of the electrical current. The boundary condition at the interface $x = 0$ is composed of two equations: the heat flux conservation Eq. (33d) and a condition of the third kind (33e). It is the latter which interests us since it expresses the temperature jump at the interface as a function of the two sought parameters R_{TC} and α.

The estimation of R_{TC} and α is based on the solution of the inverse heat conduction problem whose direct problem is given by the equations of system (33). The solution of the inverse heat conduction problem will be based on the knowledge of the following data:

- two temperature recordings within cylinder 1, denoted T^1_{m1} and T^1_{m2}, and two other temperature recordings within cylinder 2, denoted T^2_{m1} and T^2_{m2}. These measurements are located at x-coordinates: x^1_{m1}, x^1_{m2} in medium 1 and x^2_{m1} and x^2_{m2} in medium 2, respectively.
- the voltage recording (current intensity is imposed and well known).
- the electric and thermal characteristics of materials are supposed to be known, uniform and constant (Table 1) [60,61].

4.1.2. Estimation method

Let the vector to be estimated be denoted $\xi = (R_{TC}, \alpha)$. The estimation method is based on the minimization of the sum of squares criterion:

$$J(\xi) = \frac{1}{2}\sum_{k=1}^{N_t}[Y(\xi)^k - \tilde{Y}^k]^2 \tag{34}$$

where Y^k is the temperature vector calculated at time t^k at the sensor locations x^1_{m1} and x^2_{m1} · $\tilde{Y}^k$ is the temperature measured at time t^k.

One of the main problems encountered in this experiment is due to the high correlation level between R_{TC} and α. A detailed study of the sensibility coefficients has been undertaken to improve the estimation algorithm [53]. In spite of that, the accuracy of the estimations could not be improved beyond an inaccuracy of about 1% on R_{TC} and 16% on α.

4.1.3. Experimental implementation

The experimental device is presented in Fig. 9. One is interested in the interface between the two metallic cylinders of the same dimensions (a) equipped with thermocouples (b) of K type and of 80 μm diameter. Hot junctions of the thermocouples are welded at precise positions on the cylinders axis. The cylinders are laid down between two water boxes (c) which are fixed at the electrodes of the power supply (d). The water flows crossing each water box are controlled and permit to impose the desired temperatures on the boundaries of the cylinders in contact. A cold box (f) accommodates the cold junctions of the thermocouples. The temperature signals are amplified (g) before their recording by means of a fast multi-channel acquisition system (h). The electrical current is provided with a regulation system. The normal force applied to the contact is also controlled.

The model (33) is linear and considers the thermophysical properties as constant and uniform. To this end, the intensity of the current I was chosen so that the maximum heating does not exceed 50 K. We retained $I = 3000$ A. The numerical simulation allowed to choose the size of the cylinders so as to check the 1D model assumption. The latter have a diameter of 20 mm and a height of 50 mm. These dimensions ensure a uniform source term in Eq. (33a). The side surface of the cylinders is insulated massively.

The theoretical aspects of the thermocouples instrumentation in order to estimate correctly the thermal con-

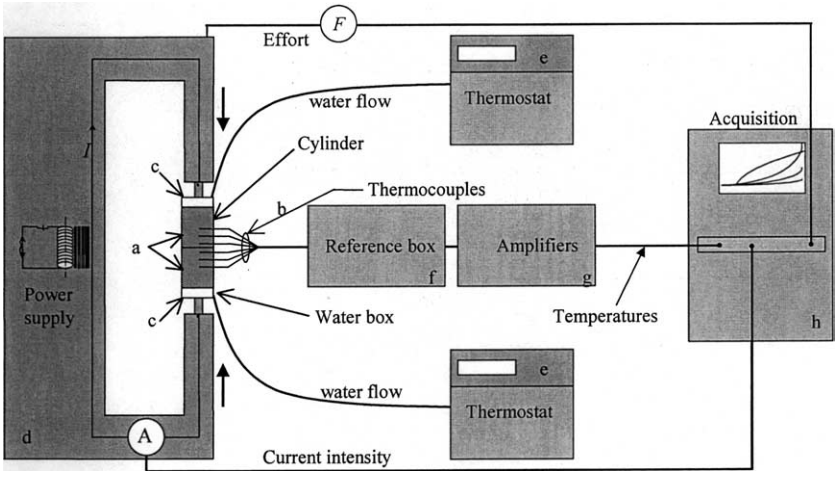

Fig. 9. Experimental setup.

tact parameters were the subject of a specific analysis [58,59]. The choice of the thermocouples positions was based on the research of the best sensitivity-precision of measurement compromise that one wishes to give to the estimations.

The experimental procedure consists in putting the two cylinders in contact between the two electrodes of the power supply and to apply a normal compression force F. In this case, we have chosen $F = 82$ daN, which corresponds to a nominal contact pressure of 2.61 MPa. The two water boxes carry water flows at the same temperature. Once the thermal steady state is reached, one switches on the electrical current which crosses the two cylinders during 4 s. Then the cylinders warm up by Joule effect. A fast acquisition system related to a cold reference box, where all the thermocouples wires are connected, permits to record the temperatures during the experiment. Before estimations of R_{TC} and α, the temperature recordings are filtered in order to eliminate the measurement noise of frequency 50 Hz due to the passage of the AC current.

The experiment is carried out six times in order to test the reproducibility of the temperature measurements and estimations. Fig. 10 presents temperature measurements related to the six experiments, and for the four thermocouples used to do the estimations. Temperature curves are monotonically increasing during the experiment. Temperature variations are more important in the steel cylinder since it is more resistive than copper. Interfacial generated heat flux being the most important heat source of the system, temperature are monotonically decreasing with distance from the interface. These results show the good superposition of the six curves related to each thermocouple, which proves the good reliability of the experiment.

The post-processing of the six experiments is done under the same numerical conditions. Table 2 gathers the results of estimations. The values of R_{TC} and α, their average values, as well as the dispersions which characterize them are presented. Table 2 contains too the value of α given by the theoretical model (26).

One notes the very weak dispersion between R_{TC} and α estimations. Posted dispersions represent only the incidences of the dispersion of the temperature measurements. The dispersion of R_{TC} and α are respectively about 0.7% and 5% of the estimated average values. That shows the good reliability of the experiment.

The estimation of R_{TC} is in accordance with the field of usually allowed values for a steel–copper contact. These results confirm the reliability of the experiment and of the estimation method. In addition, the estimation of α is about equal to the value given by the theoretical model (26). That tends to confirm the relevance of the theoretical model of α.

4.2. Case of the dynamic electrode–sheet contact during a spot welding operation [52]

The resistance spot welding process consists in joining two thin sheets maintained in contact between two copper electrodes (Fig. 11). During the welding operation, the flow of a very high current provokes fast heating of the sheets in the zone located between the two electrodes, until the melting point is reached at the sheet–sheet interface. At the microscopic scale, the current flow produces two superimposed heat sources in the asperities in contact. The first one is due to the electrical resistivities of materials. It concerns all the welding device and in particular the asperities in contact. The second one covers only the volume where electric

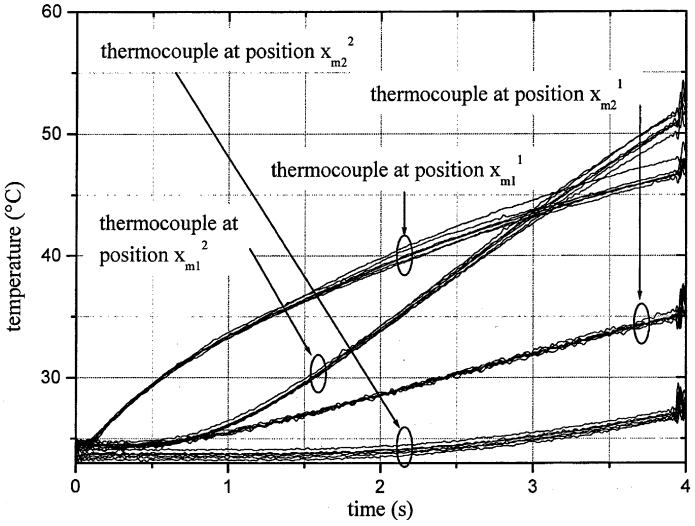

Fig. 10. Temperature measurements in the case of the steel–copper contact.

Table 2
Comparison between the analytical model and estimation results in the case of the static copper–steel contact

Test	Estimated R_{TC} (K m^2/W)	Average value of R_{TC} (K m^2/W)	δR_{TC} (K m^2/W)	Estimated α	Average value of α	$\delta\alpha$	Theoretical α (25)	Residues (°C)
1	1.42×10^{-4}			0.41				0.0098
2	1.41×10^{-4}			0.42				0.011
3	1.40×10^{-4}			0.39				0.0076
4	1.43×10^{-4}	1.41×10^{-4}	10^{-6}	0.40	0.40	2×10^{-2}	0.39	0.01104
5	1.41×10^{-4}			0.38				0.00724
6	1.39×10^{-4}			0.40				0.00109

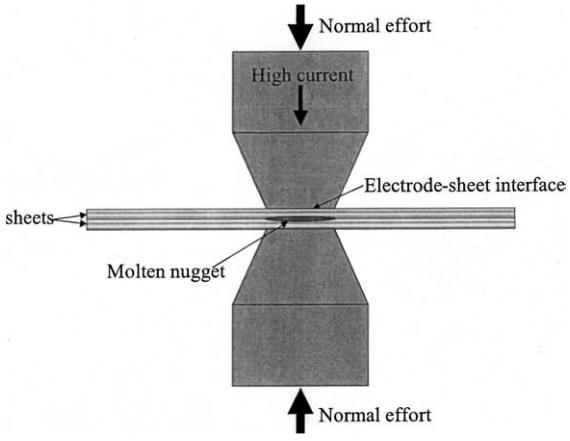

Fig. 11. Resistance spot welding process.

constrictions develop on both sides of elementary contact areas. It is important to note that the heating due to the electric micro-constriction is very fast since the characteristic time is r^2/a [54], where r is the average contact radius between asperities (∼μm), and a, the lower thermal diffusivity of the two media. The orders of magnitude do not exceed a few microseconds, and are thus insignificant in comparison with the welding time scale (0.2 s). This heating is confined to the top of the asperities. Therefore, the temperature reached in these regions is much higher than the macroscopic electrode–sheet contact temperatures. This phenomenon reduces significantly the yield stress of the softest material which is thus brought to undergo plastic deformations. This second component of the local heating has a major influence on the asperities deformations, which cause an increase in the real contact area.

The heating due to heat generation in the materials tends to dilate the sheets and the electrodes. The dilation tends to increase the compression force. However, that cannot occur because of the regulation system which maintains constant the electrode force. Thus, the significant plastic deformations of asperities in contact (spreading out of the contact), and appearance of new contacts between asperities (increase of the contact points density) are due to the decrease in the yield stress (or microhardness) of the softest material. This dynamic character related to the decreasing of the yield stress constitutes the specificity of the electro-thermal contact for a contact pressure which is maintained constant. The phenomena described above are at the origin of the contact parameters variations during a welding operation.

In a recent study [52], the heat generation factor α were experimentally estimated during a welding operation, as well as the temperatures at electrode–sheet interface. As shown in Fig. 12, α follows a time-dependent evolution. That is the consequence of the influence of the large temperature variation in the two materials in the close vicinity of the interface. Knowing evolutions of electrical resistivities and thermal conductivities of sheets and electrodes versus temperature, one can calculate α evolution from expression (26), during the welding operation. The comparison of the two curves of α is presented in Fig. 12. The two curves have comparable average values. The relative difference between model and experiment does not exceed 18% at the end of the welding operation. At $t = 0$, the two curves have the same value $\alpha = 0.5$. The curve calculated from expression (26) increases until $t = 0.0065$ s, then monotonically decreases until the end of the welding operation. On the domain $t \in [0.10\text{ s}; 0.15\text{ s}]$, the two curves are perfectly superimposed. At $t = 0.14$ s, the two curves have a common point of null derivative. The most significant variations of value between the two curves are at the beginning and the end of the welding operation.

Several reasons allow to explain the differences between the two curves. At the beginning of the welding operation, the interface structure undergoes significant and fast modifications. The duration of the local deformations could be shorter than the characteristic times of electric and thermal constrictions phenomena, what would invalidate the theoretical model. Another explanation could be related to the uncertainty on $R_{ECT/E}$ values at the beginning of the welding operation, which would introduce an error in ϕ_g calculation. It is possible that the $R_{ECT/E}$ curve used [62] does not correspond completely to the conditions of the beginning of the experiment. Lastly, Ref. [52] shows that the measurement sensitivity due to α is minimum at the beginning of the welding operation, which causes an increased

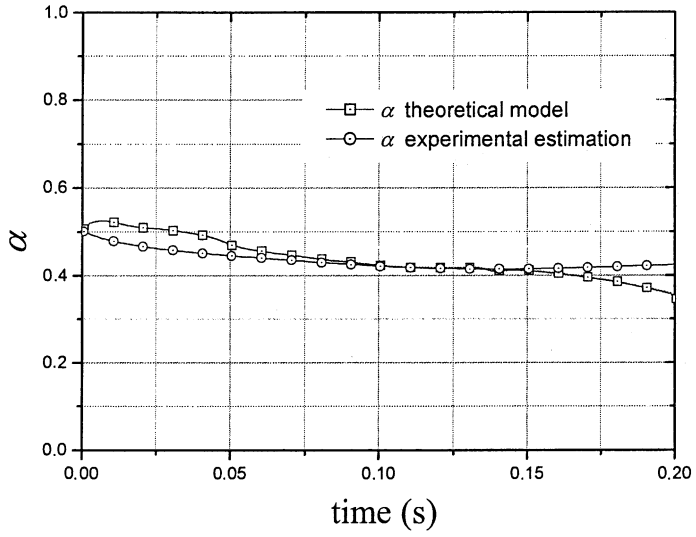

Fig. 12. Comparison between the theoretical model and estimation results in the case of the dynamic electrode–sheet interface during the spot welding process.

inaccuracy on α estimation. That could explain the differences between the two curves for $t < 0.05$ s.

At the end of the welding operation, one main phenomena occurs which could justify the difference between model and experiment for $t > 0.15$ s. Beyond that time, appearance of the molten nugget, more resistive than solid steel, causes the transfer to become slightly two dimensional in the sheet. Since the estimation algorithm is one-D, this phenomena could invalidate the estimations results at the end of the welding operation.

5. Conclusion

The heat transfer study at a solid–solid contact with an interfacial heat generation is a very interesting subject as well on the fundamental level as on that of the applications. This interest is reinforced by the growing rise of the numerical simulation which requires to know this type of contact condition.

On the basis of a microscopic model of a current tube crossing two asperities in contact, we have analysed the electrothermal diffusion phenomena in the disturbed zone, in the vicinity of the contact. The discussion, based on the assumption of semi-infinite medium, is about the partition of the generated heat flux in the constriction. This analysis leads us to define the concept of "thermal resistive path". By using the results of the microscopic analysis, a definition of the heat generation factor, noted α, is proposed in the case of a macroscopic contact. This expression of α appears as a combination of properties of the contact playing a role in heat generation and heat transfer by conduction phenomena. Thus α is independent of the thermal boundary conditions, and of the contact geometry. However, although the geometric characteristics of the contact do not appear explicitly in expression (26), they nevertheless influence the value of coefficient α. Since the contact imperfection produces a temperature discontinuity at the interface, it has an influence on the temperature level in each material, and consequently on the electrical resistivities and thermal conductivities values of which α depends.

Results of estimations of the heat generation factor in the case of a static copper–steel electro-thermal contact perfectly polished are weakly dispersed and in good agreement with the value calculated from expression (26). That indicates the good reliability of the experimental methodology, and the relevance of the theoretical model of α in the case of a static contact.

The comparison between the α curve estimated in the case of the dynamic electrothermal electrode–sheet interface during a spot welding operation and the values given by expression (26) are in good agreement. Several explanations could justify the differences between the two curves. However, the model seems to be cogency even if several improvements could be made to it, in particular with regard to the taking into account of the interface fast deformations.

References

[1] H.S. Carslaw, J.C. Jaeger, Conduction of Heat in Solids, second ed., Oxford Science Publications, 1959.
[2] V.S. Arpaci, Conduction Heat Transfer, Addison-Wesley, 1966.
[3] J.V. Beck, K.D. Cole, A. Haji-Sheikh, B. Litkouhi, Heat Conduction using Green's Functions, HPC edition, 1992.

[4] M.N. Özişik, Heat Conduction, second ed., Wiley Interscience, Ny, 1993.
[5] P. Vernotte, Thermocinétique générale, Publications scientifiques et techniques du Ministère de l'air, no. 379, Paris, 1961.
[6] K. Kato, Energy partition in conventional surface grinding, ASME Trans. J. Manufact. Sci. Eng. 121 (1999) 393–398.
[7] S. Chandrasekar, Thermal aspects of surface finishing processesSurface Engineering—ASM Handbook, vol. 5, ASM International, The Materials Information Society, USA, 1999, pp. 152–157.
[8] W. Grzesik, The role of coatings in controlling the cutting process when turning with coated indexable inserts, J. Mater. Process. Technol. 37 (1998) 133–143.
[9] L. Mazo, Contribution à l'étude thermocinétique du frottement métal-plastique, Thèse de doctorat, Université de Nantes, 1977.
[10] L. Mazo, B. Cassagne, D. Badie-Levet, J.P. Bardon, Etude des conditions de liaison thermique dans le cas du frottement sec métal-plastique, Revue Générale de Thermique (204) (1978) 919–933.
[11] A.A. Yevtushenko, The applicability of hereditary model of wear with an exponential kernel in the one-dimensional contact problem taking frictional heat generation into account, J. Appl. Maths. Mech. 3 (5) (1999).
[12] R. Kulchytsky-Zhyhailo, Axi-symmetric contact problem with frictional heating for thermally non-linear sliders, Int. J. Mech. Sci. 40 (11) (1998) 1133–1143.
[13] R. Kulchytsky-Zhyhailo, A simplified solution for three-dimensional contact problem with heat generation, Int. J. Eng. Sci. 39 (2001) 303–315.
[14] V. Pauk, Periodical contact problems for a half-space involving frictional heating, Int. J. Mech. Sci. 39 (1) (1997) 87–95.
[15] V. Pauk, Plane contact problem for a layer involving frictional heating, Int. J. Heat Mass Transfer 42 (1999) 2583–2589.
[16] A.A. Yevtushenko, Effect of the rough surface on the transient frictional temperature and thermal stresses near a single contact area, Wear 197 (1996) 160–168.
[17] A.A. Yevtushenko, Approximate solution of the thermo-elastic contact problem with frictional heating in the general case of the profile shape, J. Mech. Phys. Solids 40 (2) (1996) 243–250.
[18] D.V. Grylitsky, Some quasi-stationary contact problems for half-space involving heat generation and radiation, Int. J. Eng. Sci. 33 (12) (1995) 1773–1781.
[19] A.A. Yevtushenko, Axi-symmetrical transient contact problem for sliding bodies with heat generation, Int. J. Solids Struct. 32 (16) (1995) 2369–2376.
[20] A.A. Yevtushenko, Determination of limiting radii of the contact area in axi-symmetric contact problems with frictional heat generation, J. Mech. Phys. Solids 43 (4) (1995) 599–604.
[21] A.A. Yevtushenko, About interaction of frictional heat generation and wear on transient axi-symmetrical contact of sliding, Int. J. Eng. Sci. 33 (5) (1995) 625–632.
[22] A.A. Yevtushenko, The interaction of frictional heating and wear at a transient sliding contact, J. Appl. Math. Mech. 59 (3) (1995) 459–466.
[23] A.M. Al-Shabibi, transient solution of a thermo-elastic instability problem using a reduced order model, Int. J. Mech. Sci. 44 (2002) 451–464.
[24] A.D. Dimarogonas, A compilation of heat distribution parameters at sliding contacts, Tribol. Int. 2 (1981) 225–229.
[25] K. Varadi, Evolution of the real contact areas, pressure distribution and contact temperatures during sliding contact between real metal surfaces, Wear 200 (1996) 55–62.
[26] R. Kulchytsky-Zhyhailo, Thermo-elastic contact problems with frictional heating and convective cooling, Int. J. Eng. Sci. 35 (3) (1997) 211–219.
[27] R. Komanduri, Thermal modelling of the metal cutting process, Int. J. Mech. Sci. 43 (2001) 57–88.
[28] R. Komanduri, Analysis of heat partition and temperature distribution in sliding systems, Wear 251 (2001) 925–938.
[29] R. Komanduri, Thermal analysis of dry sleeve bearings—a comparison between analytical, numerical (finite element) and experimental results, Tribol. Int. 34 (2001) 145–160.
[30] V.P. Levytskyi, Plane contact problem with heat generation account of friction, Int. J. Eng. Sci. 34 (1) (1996) 101–112.
[31] V.P. Levytskyi, The unsteady axi-symmetric contact problem with heat generation, Int. J. Math. Mech. 61 (5) (1997) 843–850.
[32] A.A. Yevtushenko, The non-stationary contact problem for rough bodies taking heat generation by friction into account, Int. J. Math. Mech. 60 (4) (1996) 687–692.
[33] M. Ciavarella, Interaction of thermal contact resistance and frictional heating in thermo-elastic instability, Int. J. Solids Struct. 40 (2003) 5583–5597.
[34] G.C. Barber, Distribution of heat between sliding surfaces, J. Mech. Eng. Sci. 9 (1967) 351–354.
[35] L. Johansson, Model and numerical algorithm for sliding contact between two elastic half-planes with frictional heat generation and wear, Wear 160 (1993) 77–93.
[36] H.A. Abdel Aal, On the bulk temperatures of dry rubbing metallic solid pairs, Int. Comm. Heat Mass Trans. 26 (4) (1999) 587–596.
[37] J.P. Bardon, Bases physiques des conditions de contact thermique imparfait entre deux milieux en glissement relatif, Revue Générale de Thermique 386 (1994) 85–91.
[38] P. Chantrenne, M. Raynaud, A microscopic thermal model for dry sliding contact, Int. J. Heat Mass Transfer 40 (5) (1997) 1083–1094.
[39] N. Laraqi, Température de contact et coefficient de partage du flux généré par frottement sec entre deux solides. Approche nouvelle de la génération de flux, Int. J. Heat Mass Transfer 35 (11) (1992) 3131–3139.
[40] J.-G. Bauzin, N. Laraqi, Estimation of thermal contact parameters at the interface between two sliding solids, in: Proceedings of Eurotherm 68, Poitiers, 2001.
[41] J.-G. Bauzin, N. Laraqi, Experimental determination of the thermal contact resistance and the local heat partition coefficient at the interface of two solids in dry friction, in: Proceedings of 12th IHTC, Grenoble, 2002, pp. 27–32.
[42] R. Holm, Electric Contacts—Theory and Application, fourth ed., Springer, Berlin, 1967.
[43] J.A. Greenwood, Temperatures in spot welding, British Welding Journal 8 (6) (1961) 316–322.
[44] F.P. Bowden, Electrical conduction in solids—I. Influence of the passage of current on the contact between solids, Proc. Royal Soc. Lond. 246 (1958) 1–12.

[45] G. Le Meur, Mesure de la résistance thermique de contact à l'interface tôle-électrode lors d'une opération de soudage par point, in: Proceedings Congrès SFT, Vittel, 2002.
[46] G. Le Meur, Etude de la condition de liaison thermique à une interface de contact solide–solide siège d'une dissipation par effet Joule: application au soudage par résistance, Thèse de Doctorat, Université de Nantes, 2002.
[47] Y.J. Cho, An analysis of the transient nugget formation in resistance spot welds, Proc. Instn. Mech. Engrs. 200 (B3) (1986) 167–172.
[48] Z. Han, Resistance spot welding: a heat transfer study, Welding J. 68 (9) (1989) 363–371.
[49] H.S. Cho, A steady of the thermal behaviour in resistance spot welding, Welding J. 68 (6) (1989) 236–244.
[50] J.A. Khan, Numerical simulation of resistance spot welding process, Numer. Heat Transfer, Part A (37) (2000) 425–446.
[51] P.C. Wang, Modeling dynamic electrical resistance during resistance spot welding, Trans. ASME 123 (2001) 576–585.
[52] G. Le Meur, B. Bourouga, T. Dupuy, Measurement of contact parameters at electrode–sheet interface during resistance spot welding process, Sci. Technol. Welding Joining 8 (6) (2003) 415–422.
[53] G. Le Meur, B. Bourouga, Y. Jarny, Inverse analysis of heat flow at a solid electro-thermal contact, 4th International Conference of Inverse Problems in Engineering, Rio de Janeiro, Brazil, 2002.
[54] J.P. Bardon, B. Cassagne, B. Fourcher, C. Saint-Blanquet, Bilan des principales recherches sur les résistances de contact, Rapport DETB 7101, Lab. Thermocinétique, Université de Nantes, 1971.
[55] M.G. Cooper, A note on electrolytic analogue experiments for thermal contact resistance, Int. J. Heat Mass Transfer 12 (12) (1969) 1715–1718.
[56] T. Hisakado, On the mechanism of contact between solid surfaces, Bull. JSME 2 (54) (1969) 1519–1545.
[57] G. Le Meur, B. Bourouga, J.P. Bardon, Etude théorique des mécanismes de base du transfert de chaleur à travers une interface siège d'une dissipation par effet joule, Actes du Congrès SFT, Nantes, Ed. Elsevier, 2001, pp. 653–658.
[58] B. Bourouga, Les aspects théoriques régissant l'instrumentation d'un capteur thermique pariétal à faible inertie, Int. J. Therm. Sci. 39 (2000) 96–109.
[59] A. Sorin, Etude Numérique du caractère intrusif de l'instrumentation pariétale par thermocouple, Congrès Annuel de la SFT, Vittel, 2002.
[60] ASM Handbook: Properties and Selection: Non-Ferrous Alloys and Pure Elements, 10th ed., vol. 2, 1979.
[61] ASM Handbook: Properties and Selection: Irons, Steels, and High Performance Alloys, 10th ed., vol. 1, 1990.
[62] E. Thieblemont, Modélisation du soudage par résistance par point, Thèse de doctorat, Inst. Polytechnique de Lorraine, 1992.